

## Mechanical stability of Pd-H systems: A molecular-dynamics study

W. Zhong, Y. Cai,\* and D. Tománek†

*Department of Physics and Astronomy, Michigan State University, East Lansing, Michigan 48824-1116  
and Center for Fundamental Materials Research, Michigan State University, East Lansing, Michigan 48824-1116*

(Received 17 April 1992)

We use the Nosé and Rahman-Parrinello molecular-dynamics formalism to study the equilibrium structure and elastic properties of bulk Pd as a function of temperature and hydrogen concentration. Introducing tensile stress as an independent variable into this formalism enables us also to study the elastic breakdown and crack formation as a function of a uniaxially applied load. The calculations are performed using a model many-body alloy Hamiltonian based on *ab initio* density-functional results for Pd-H systems. Our results indicate that the microscopic origin of "hydrogen embrittlement" is an increased *ductility* and *plasticity* in regions saturated by hydrogen, in agreement with the postulated hydrogen-enhanced local-plasticity mechanism.

### I. INTRODUCTION

Studies of the mechanical stability of transition metals that are exposed to hydrogen are of great interest to both basic sciences and technology. On most transition metals of interest, hydrogen molecules adsorb dissociatively. Hydrogen atoms diffuse relatively freely into the bulk metal, where they can reduce the mechanical stability of the system significantly.<sup>1</sup> The microscopic origin of this effect, which is known as hydrogen embrittlement,<sup>2</sup> is presently not well established. Nevertheless, hydrogen embrittlement causes extensive engineering difficulties, e.g., when considering hydrogen storage in metals, construction of stable fusion reactors and underwater structures, and space technology. Several fundamental questions have remained unanswered. Very little is known about the atomic-level response to applied tensile stress, to temperature changes, and to hydrogen loading of bulk metals. The study of these effects is expected to answer some key questions related to macroscopic materials properties, especially hydrogen embrittlement.

The most straightforward way to address the above questions is to use a molecular-dynamics (MD) technique. Such a calculation describes the evolution of the system with time, based on a direct numerical solution of the equations of motion for individual atoms. This procedure goes beyond lattice dynamics<sup>3</sup> which is limited to small atomic displacements and cannot address problems such as the melting transition or fracture. The appropriate MD technique for these questions will describe the dynamics of the system at constant nonzero temperatures using a canonical ensemble and can model the response of a system to an externally applied tensile stress.<sup>4</sup> Such a simulation provides microscopic information about the dynamics of the system, including structural changes during phase transitions (such as melting or stability breakdown due to increased temperature or the presence of hydrogen). Of critical importance for a successful description of these phenomena is a precise and computer efficient description of interatomic interactions.

Different kinds of model potentials have been used in

MD simulations, including simple isotropic pair potentials, more complex parametrized potentials with angular forces, and many-body potentials.<sup>4</sup> Clearly, the most desirable approach would be to use first-principles total energy functionals directly.<sup>5</sup> Since realistic MD simulations are to consider large ensembles over long-time periods, it is imperative to emphasize simplicity and minimize the reduction of accuracy. Recently, the embedded-atom method<sup>6</sup> (EAM) has been used in MD studies of the structure and dynamics of metals.<sup>7</sup> Owing to its efficiency and universal set of parameters describing a given element in the periodic system, EAM has proven to be a very successful method to generate interatomic potentials which can be used in MD studies. While the EAM works best in single-component systems for which the element-specific parameters have been optimized, the corresponding results for multicomponent systems are generally less reliable. More recently, we developed a model many-body alloy (MBA) potential,<sup>8</sup> which is quite general in nature, easy to handle numerically, and which is based on *ab initio* calculations for alloy systems. We have used this potential successfully to predict the equilibrium structure and dynamics of bulk Pd and clean as well as hydrogen-covered Pd surfaces at zero temperature.<sup>8</sup>

In the present paper, we will use the MBA potential in a MD study of the effect of hydrogen and temperature changes on the mechanical properties of metals. As in Ref. 8, we will focus on Pd. This transition metal shows a large variety of interesting effects when exposed to hydrogen, such as hydride formation and surface reconstruction, and has been studied extensively by first-principles techniques.<sup>9-11</sup> We will show that both temperature and H loading affect the elastic constants of bulk Pd significantly. This is true especially for the critical tensile stress required to form a crack, which decreases steadily with increasing temperature and hydrogen concentration.

This paper is structured as follows. In Sec. II, we briefly review the method used to evaluate the total energy of the Pd-H system and summarize the molecular dynamics formalism as applied to this system under tensile stress. In Sec. III, we present results for the equi-

librium structural and elastic properties of Pd at different temperatures and hydrogen concentrations, and show quantitative results for the elastic breakdown and crack formation in hydrogen-free and hydrogen-loaded Pd as a function of uniaxially applied load. These results are discussed in Sec. IV. Finally, in Sec. V, we summarize our results and present general conclusions.

## II. THEORY

### A. Evaluation of the potential energy

We determine the potential energy of the Pd-H system using the many-body alloy Hamiltonian.<sup>8</sup> This is a computationally efficient scheme, which has been successfully used previously to study the electronic and structural properties of small clusters, surfaces of metals, and dilute metal alloys.<sup>12–15</sup> As discussed earlier,<sup>12–14</sup> the total potential energy  $V$  of the crystal can be decomposed into individual atomic binding energies  $E_{\text{coh}}(i)$ , which have an attractive part  $E^{BS}(i)$  due to the hybridization of orbitals, and a part  $E^R(i)$  describing repulsive interactions. We obtain

$$\begin{aligned} V &= \sum_i E_{\text{coh}}(i) \\ &= \sum_i E^{BS}(i) + E^R(i). \end{aligned} \quad (1)$$

We base the expression for  $E^{BS}$  on a parametrized tight-binding Hamiltonian and the second-moment approximation, and assume an exponential distance dependence for both the hopping integrals and the pairwise repulsive interactions in  $E^R$ . For systems with more than one component (such as alloys and compounds), the binding energy of atom  $i$  in Eq. (1) is given by

$$\begin{aligned} E_{\text{coh}}(i) &= - \left\{ \sum_{j \neq i} \xi_{0,\alpha\beta}^2 \exp \left[ -2q_{\alpha\beta} \left( \frac{r_{ij}}{r_{0,\alpha\beta}} - 1 \right) \right] \right\}^{1/2} \\ &\quad + \sum_{j \neq i} \epsilon_{0,\alpha\beta}^R \exp \left[ -p_{\alpha\beta} \left( \frac{r_{ij}}{r_{0,\alpha\beta}} - 1 \right) \right]. \end{aligned} \quad (2)$$

Here, we assume that the atom  $i$  is of type  $\alpha$  and that the summation extends over its neighbors  $j$  of type  $\beta$ .  $r_{ij}$  is the distance between these atoms and  $r_{0,\alpha\beta}$  is the corresponding equilibrium distance. We use the Greek indices to denote the atom type, i.e., Pd or H.

In the MBA Hamiltonian, each of the H-H, H-Pd, and Pd-Pd interactions is characterized by a set of five parameters. These are the hopping integral  $\xi_0$  and the pairwise repulsive energy  $\epsilon_0^R$ , both given at the equilibrium distance  $r_0$ . The distance dependence of  $\xi$  and of  $\epsilon^R$  is described by the parameters  $q$  and  $p$ , respectively. The values of these parameters have been obtained by a careful fit<sup>8</sup> to corresponding *ab initio* calculations<sup>11</sup> for bulk Pd and PdH and are listed in Table I. The formal simplicity of Eq. (2) makes it easy to determine the sensitivity of the results on these parameters. The energy depends in a linear fashion on  $\xi_0$  and  $\epsilon_0^R$ . The parameter  $r_0$  fixes the lattice constant, and the bulk modulus  $B$  is proportional to the product  $qp$ . The assumption of

TABLE I. Interaction parameters used in the many-body alloy Hamiltonian for the Pd-H system.

Interaction	$q_{\alpha\beta}$	$p_{\alpha\beta}$	$r_{\alpha\beta,0}$ (Å)	$\epsilon_{\alpha\beta}^R$ (eV)	$\xi_{\alpha\beta}$ (eV)
Pd-Pd	3.40	14.8	2.758	0.08376	1.2630
H-H	3.22	5.28	2.300	0.1601	0.9093
H-Pd	2.20	5.50	1.769	0.6794	2.5831

isotropic hopping integrals in Eq. (2), which is justified for the near noble-metal electronic configuration of Pd, simplifies our calculations considerably. While it does not affect the stability of close-packed structures such as Pd and PdH, it may result in too low values of the shear moduli in metals with an open  $d$  shell.<sup>16</sup>

We found the results for the lattice constants, cohesive energies, and the bulk moduli of the bulk systems, as obtained using the MBA method, to be in good agreement with the LDA results and experimental data.<sup>8</sup> This indicates that Eq. (2) has sufficient flexibility to describe the energy and the dynamics of the Pd-H system accurately.

### B. Molecular-dynamics formalism

The dynamics of an isolated  $N$ -particle system in three-dimensional space is governed by the Lagrangian

$$L = \sum_{i=1}^N \frac{1}{2} m_i \dot{\mathbf{q}}_i^2 - V(\{\mathbf{q}_i\}). \quad (3)$$

Here,  $\mathbf{q}_i$  is the position vector of atom  $i$  in the system and  $V(\{\mathbf{q}_i\})$  is the total potential energy, given by Eqs. (1) and (2). The dynamical evolution of the system is described by Euler-Lagrange equations derived from the above Lagrangian. This procedure yields statistics for a microcanonical ensemble. Unfortunately, the simulation of a realistic microcanonical system requires a very large number of particles which imposes unrealistic requirements on the computation.

A more natural choice is the canonical ensemble, which considers the temperature (rather than the total energy) to be constant, and which allows for a free-energy exchange with the external heat bath. We use an algorithm due to Nosé<sup>17</sup> to describe a canonical ensemble. In the Nosé scenario, the fixed temperature canonical ensemble can be simulated by considering a single additional variable  $s$ . In this extended phase space, the net effect of the heat bath is assumed to be a scaling of the velocities as  $\mathbf{v}_i = s \dot{\mathbf{q}}_i$ . Nosé interpreted the scaled velocity  $\mathbf{v}_i$  as the true velocity resulting from the heat exchange with the external heat bath. The canonical ensemble can be described in an augmented Lagrangian of the form

$$L = \sum_{i=1}^N \frac{1}{2} m_i s^2 \dot{\mathbf{q}}_i^2 - V(\{\mathbf{q}_i\}) + \frac{1}{2} Q \dot{s}^2 - (N_f + 1) T_{\text{eq}} \ln s. \quad (4)$$

Here,  $N_f = 3N$  is the number of degrees of freedom

of the system.  $Q$  is the mass associated with the new variable  $s$  which describes the coupling to the external heat bath.  $T_{\text{eq}}$  is the temperature of the heat bath and consequently the equilibrium temperature of the system. The optimum choice of  $Q$  provides an efficient damping of the equilibrium state. Overdamping is avoided by choosing  $Q$  in such a way that the oscillation period of  $s$  is much smaller than the damping time constant. The Lagrangian in Eq. (4) contains a logarithm of  $s$  in the potential-energy part which makes this extended system equivalent to the canonical ensemble describing the original  $N$ -particle system. This new Lagrangian is justified by the correct statistics it yields for the system. In other words, when integrating the partition function over the new dimension in phase space, we regain the partition function for the canonical ensemble. Consequently, the microcanonical ensemble of the augmented Lagrangian, described by Eq. (4), generates precisely the canonical ensemble of the original  $N$ -particle system.

In order to describe the effect of mechanical coupling between the ensemble and the outside world, Andersen applied molecular dynamics to systems under constant hydrostatic pressure.<sup>18</sup> In this technique, the variable space is extended by an additional quantity which scales all the atomic coordinates in the unit cell, thus allowing the volume to change uniformly. This method can be combined with Nosé's treatment of the canonical ( $TN$ ) ensemble to describe the behavior of that system at constant tensile stress (or tension)  $t$  ( $TtN$  ensemble). This method has been further generalized by Parrinello and Rahman<sup>19</sup> to allow for anisotropic stress and corresponding shape changes of the unit cell.

The mechanical stability of Pd and PdH systems is intimately related to the dynamics of these systems under uniaxial tensile stress. In this paper, we study this process using the method of Parrinello and Rahman.<sup>19</sup> In our molecular-dynamics calculations, we consider a unit cell which is spanned by the three Bravais lattice vectors  $\mathbf{a}$ ,  $\mathbf{b}$ , and  $\mathbf{c}$ . These vectors define a shape matrix  $\underline{h} = (\mathbf{a}, \mathbf{b}, \mathbf{c})$  which is used to describe the response of the system to applied stress. This matrix maps the true atomic coordinates onto reduced coordinates  $\mathbf{q}_i$  which lie in a cube of unit length, so that the true coordinates are obtained by the scaling transformation  $\underline{h}\mathbf{q}_i$ . The Lagrangian describing the  $TtN$  ensemble is then given by

$$L = \sum_{i=1}^N \frac{1}{2} m_i s^2 (\mathbf{q}_i^T \underline{G} \mathbf{q}_i) - V(\{\mathbf{q}_i\}) + \frac{1}{2} Q \dot{s}^2 - (N_f + 1) T_{\text{eq}} \ln s + \frac{1}{2} W_t \text{Tr}(\dot{\underline{h}}^T \dot{\underline{h}}) - V_0 \text{Tr}(\underline{t} \underline{\epsilon}). \quad (5)$$

The first term describes the kinetic energy of the system, and the matrix  $\underline{G}$  is given by  $\underline{G} = \underline{h}^T \underline{h}$ .  $W_t$  is the mass of the "piston" which exerts the external tension on the system. The equilibrium volume of the MD unit cell at zero tension is denoted by  $V_0$  and the equilibrium shape by  $\underline{h}_0$ . In the case of nonzero tension, we define a strain matrix  $\underline{\epsilon}$  by

$$\underline{\epsilon} = \frac{1}{2} [(\underline{h}_0^{-1})^T \underline{G} \underline{h}_0^{-1} - \underline{I}]. \quad (6)$$

The quantity  $\underline{t}$  in Eq. (5) is the thermodynamic tension tensor which gives the work  $dW$  due to an infinitesimal distortion of the system as  $dW = V_0 \text{Tr}(\underline{t} \underline{\epsilon})$ .  $\underline{t}$  is related to the stress tensor  $\underline{\sigma}$  by<sup>19</sup>

$$\underline{\sigma} = V_0 \underline{h} (\underline{h}_0^{-1}) \underline{t} (\underline{h}_0^{-1})^T \underline{h}^T / V, \quad (7)$$

where  $\underline{h}$  is the average value of the shape matrix and  $V = \det(\underline{h})$  is the average volume.

Once the Lagrangian  $L$  is established, the equations of motion are given by

$$\begin{aligned} \frac{d}{dt} \left( \frac{\partial L}{\partial \dot{q}_{i\alpha}} \right) - \left( \frac{\partial L}{\partial q_{i\alpha}} \right) &= 0, \\ \frac{d}{dt} \left( \frac{\partial L}{\partial \dot{h}_{\alpha\beta}} \right) - \left( \frac{\partial L}{\partial h_{\alpha\beta}} \right) &= 0, \\ \frac{d}{dt} \left( \frac{\partial L}{\partial \dot{s}} \right) - \left( \frac{\partial L}{\partial s} \right) &= 0. \end{aligned} \quad (8)$$

Here, we have used Greek indices to denote the vector and matrix components of  $\mathbf{q}_i$  and  $\underline{h}$ , respectively.

The dynamics of the system is obtained by integrating the equations of motion in real time using a predictor-corrector method of fifth order.<sup>20</sup> The typical time step in the MD calculation of bulk Pd is  $2 \times 10^{-15}$  s. For hydrogen loaded Pd, the time step is reduced to  $5 \times 10^{-16}$  s due to the high vibration frequency and large-scale diffusion of the light hydrogen atoms. The generalized energy of the system is a constant of motion. We control the numerical fluctuations of this quantity (due to the finite time steps) to lie within a small error margin of  $10^{-4}$ , which is indicative of a precise integration. In order to avoid overdamping, we tune the mass  $Q$  associated with the temperature and the mass  $W_t$  associated with the tensile stress in such a way that the fluctuations of temperature and volume occur over large periods of  $\approx 50$ – $100$  time steps. In a typical MD calculation, we consider a periodic arrangement of unit cells (with originally cubic shape) which contain 500 Pd atoms and a fixed number of hydrogen atoms. When studying the properties of the system at a specific temperature or pressure, we first let the system equilibrate over a period of  $\approx 30\,000$  time steps and only then start collecting data for statistics. We find this time period to be sufficient for excellent statistics with negligible error bars.

In the derivation of the algorithm, Nosé has assumed the system to be ergodic.<sup>17</sup> Doubts have been raised about the validity of this assumption,<sup>21</sup> especially in the case of small systems. There are two reasons why this criticism should not affect our results. First, we consider a very large system with more than 1500 degrees of freedom. Second, the many-body alloy potential contains anharmonic terms which gain importance at interatomic distances substantially different from  $r_0$ . Especially at elevated temperatures, this fact contributes to a fast onset of chaotic behavior.

### III. RESULTS

#### A. Thermal expansion and melting transition in Pd

The first nontrivial application of our formalism is to determine the equilibrium volume of Pd as a function of temperature, and to study the melting transition. In the corresponding molecular-dynamics simulation, we consider an originally cubic volume (or simulation box) containing 500 Pd atoms on a fcc lattice. Periodic boundary conditions are used to eliminate surface effects, and the external pressure is set to zero. We start our simulation by first equilibrating the system for 10 000 time steps (corresponding to  $2 \times 10^{-11}$  s) in a  $VtN$  canonical ensemble which is in contact with a heat bath at  $T = 300$  K. This simulation is followed by another 20 000 time steps in the  $TtN$  canonical ensemble at zero external pressure. The equilibrium volume  $V$  per atom is related to the volume of the simulation box, and is obtained from a running average during the simulation. The statistical error based on the last 10 000 time steps is found to be negligible. After  $V$  has been determined for the given temperature, the heat bath is gradually warmed up to another temperature, and the equilibrium volume per atom is obtained from a statistical average over 10 000 time steps at the new temperature.

Our results, presented in Fig. 1(a), indicate a thermal expansion of the lattice in the whole temperature range studied. In the temperature range between  $T = 2000$ – $2050$  K, the equilibrium volume per Pd atom shows a discontinuous increase, indicative of a first-order phase transition. This phase transition corresponds to the melting point, as can be verified by inspecting the trajectories of individual Pd atoms at temperatures below and above the critical temperature, shown in Figs. 2(b) and 2(c). Near the melting point, our calculations show a narrow hysteresis describing an overheated solid or an undercooled liquid, depending on whether the system is being heated or cooled. The difference of  $\lesssim 10\%$  between the calculated melting temperature and the experimental value<sup>24</sup> of  $T_M = 1827$  K is impressively small in view of the fact that our interaction potentials are based on  $T = 0$  static properties of Pd. A small positive difference between the calculated and the observed melting point is also expected due to the finite size of the unit cell.

In the temperature range  $T < 1500$  K, the thermal expansion of the lattice is nearly linear, corresponding to a thermal (linear) expansion coefficient of  $\alpha_l = 1.7 \times 10^{-5} \text{ K}^{-1}$ . While we could not find any corresponding experimental results for Pd, our value lies very close to  $\alpha_l = 1.89 \times 10^{-5} \text{ K}^{-1}$  which has been observed in Ag,<sup>22</sup> a neighbor of Pd in the periodic system. At higher temperatures, the volume-temperature relation shows strong deviations from linearity. This relationship bears information about the Pd-Pd interaction potentials at large interatomic separations. Above the melting point, the expansion coefficient of the system experiences an abrupt increase above the solid phase value, correlated with a sharp increase of the interparticle distance at  $T_M$ .

In order to illustrate the effect of temperature on the dynamical behavior of the system, we showed the trajec-

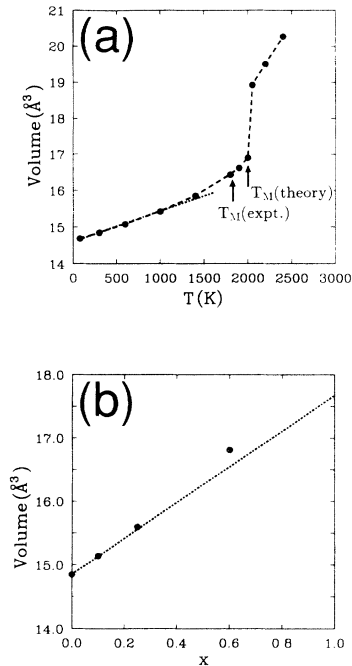


FIG. 1. (a) Equilibrium volume  $V$  of a Pd atom in bulk Pd as a function of temperature  $T$ . The dashed line is a guide to the eye connecting the calculated data points. Observed linear expansion of Ag (Ref. 22), the neighboring element of Pd, is shown by the dotted line. (b) Equilibrium volume  $V$  per Pd atom in bulk  $\text{PdH}_x$ , as a function of the hydrogen concentration  $x$ . The dotted line corresponds to the observed (Ref. 23) expansion coefficient of Pd as a function of  $x$ . Our molecular-dynamics results are given by solid circles in (a) and (b).

tories of individual Pd atoms [projected onto the (100) plane] in Figs. 2(a)–2(c) at different temperatures. At  $T = 300$  K, all atoms appear to be pinned to their equilibrium site and show negligible fluctuations about this position, reflected in a very small Debye-Waller factor.

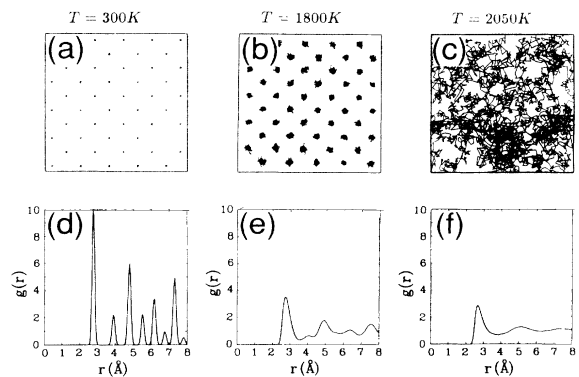


FIG. 2. Atomic trajectories in bulk Pd at the temperatures (a)  $T = 300$  K and (b)  $T = 1800$  K below the melting temperature  $T_M$ , and (c) at  $T = 2050$  K above  $T_M$ . Corresponding pair correlation functions  $g(r)$  at  $T = 300$ , 1800, and 2100 K are shown in (d), (e), and (f), respectively.

At  $T = 1800$  K, the fluctuations of Pd atoms about their equilibrium sites are already quite appreciable. The size of these fluctuations is a considerable fraction of the lattice constant, which, according to Lindemann's criterion, is indicative of the proximity to the melting point. A statistically negligible fraction of atoms is also seen to diffuse far away from their site, but the crystalline order still exists. Above the melting point, all atoms diffuse relatively freely throughout the sample, as shown in Fig. 2(c), and the long-range order is destroyed.

A more quantitative measure of the crystalline order is the pair correlation function  $g(r)$  which is shown in Figs. 2(d)–2(f) for the above temperature values. Clearly, the validity of conclusions related to the long-range order in the crystal is limited by the finite size of the simulation box. At  $T = 300$  K,  $g(r)$  consists of a set of sharp peaks which will result in a sharp diffraction pattern. At  $T = 1800$  K,  $g(r)$  still shows a substantial amount of structure even for large interatomic distances  $r$ , indicative of long-range order, but the peaks are smeared out and begin to overlap. Above the melting transition, the most characteristic feature in the pair correlation function is a peak at the nearest-neighbor distance. For larger

interatomic distances,  $g(r)$  contains almost no information about the atomic structure and approaches the constant value  $g(r) = 1$  very rapidly. This would justify a treatment of the liquid as a continuous medium beyond the nearest-neighbor distance.

As we will discuss later on in connection with fracture, interesting details about the cohesion of the system under different conditions can be learned from the distribution of atomic binding energies. In Figs. 3(a) and 3(b), we compare the binding energy distribution for bulk Pd atoms at  $T = 300$  and  $2100$  K, just above the melting point. In absence of applied tensile stress, our simulations indicate that binding energies in the system can be characterized by a rather featureless single-peaked distribution function indicating that most atoms have an indistinguishable environment. The small width of this peak at  $T = 300$  K, shown in Fig. 3(a), reflects an almost perfect crystalline order at this temperature. Above the melting point, this peak is strongly broadened and shifted towards smaller binding energies, as shown in Fig. 3(b). The former effect comes from the large variety of binding sites in the liquid; the latter one reflects the loss of cohesion mainly due to a uniform lattice expansion.

## B. Mechanical stability of Pd under tensile stress

One of the most challenging problems related to the mechanical stability of metals is to obtain a quantitative understanding of the fracture process due to uniaxially applied tensile stress. We address this problem by studying the deformation of a metal block (the simulation box) under a uniaxial load, as shown schematically in Fig. 4(a). We expect the length  $z$  of the metal block first to increase monotonically with increasing load. Once a critical value of the tensile stress  $p_c$  is reached, the material can no longer support the load and breaks into parts. In the following, we describe the molecular-dynamics simulation of the elastic and plastic deformations in the Pd metal block which is exposed to increasing uniaxial tensile stress, as a function of temperature and — in the following subsection — as a function of hydrogen concentration.

In our MD simulation, we consider a canonical ( $TtN$ ) ensemble of 500 Pd atoms in a simulation box which has cubic shape at zero applied stress, but which can vary its shape freely in the case of anisotropic pressure. For a given temperature of the heat bath, we determine the shape changes [especially the elongation of the cell  $\Delta z$ , see Fig. 4(a)] in response to uniaxial tensile stress which is described by the stress matrix

$$\sigma = \begin{pmatrix} 0 & 0 & 0 \\ 0 & 0 & 0 \\ 0 & 0 & p \end{pmatrix}. \quad (9)$$

Our results for the elongation  $\Delta z$  of the MD unit cell as a function of  $p$  are shown in Fig. 4(b) for temperatures between 77 and 1800 K. In our simulation, we increased the uniaxial stress  $p$  in finite steps of initially  $\Delta p = 2.0$  GPa from zero to a load just below the point of fracture. From there on, we decreased  $\Delta p$  to 0.5–1 GPa

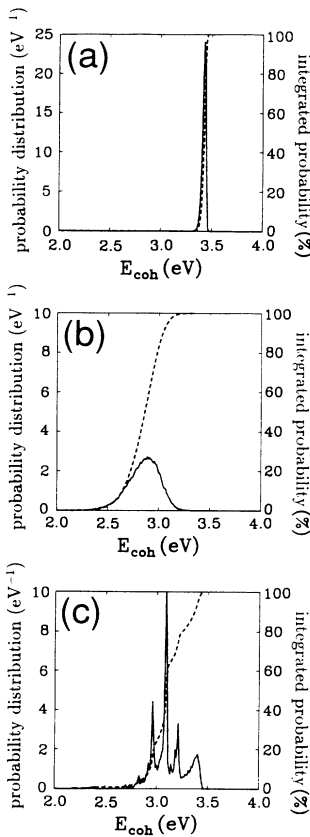


FIG. 3. Distribution of atomic binding energies  $E_{\text{coh}}$  in bulk Pd at (a)  $T = 300$  K and (b)  $T = 2100$  K at zero pressure. (c) Corresponding data for Pd at  $T = 300$  K at the point of critical uniaxial tensile stress  $p_c$  for breakdown [compare with Fig. 4(b)]. The solid lines give the probability distribution, the dashed lines show the integrated probability.

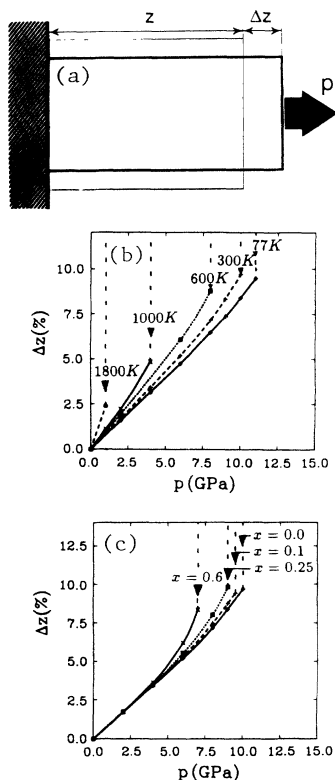


FIG. 4. (a) Schematic picture of Pd deformations under tensile stress, showing the length  $z$  and deformation  $\Delta z$  of the unit cell. (b) Deformation  $\Delta z$  of bulk Pd as a function of the external tensile stress  $p$ , for different temperatures. (c) Deformation  $\Delta z$  of hydrogen-loaded bulk Pd at  $T = 300$  K, as a function of the external tensile stress  $p$ , for different hydrogen concentrations. Our molecular dynamics results are given by the data points. The lines are guides to the eye.

in order to increase the accuracy of the calculated critical tensile stress  $p_c$ . At each value of  $p$ , the system has been allowed typically 5000 time steps (or  $10^{-11}$  s) to equilibrate. We observed that the equilibration takes longer near the point of fracture and extended the simulation accordingly. The equilibrium shape of the MD unit cell has been obtained by averaging over the last 5000 time steps.

The first important result of our simulation is the order of magnitude for the critical tensile stress  $p_c$  to initiate fracture, typically a few GPa. As shown in Fig. 4(b),  $p_c$  decreases with increasing temperature, from 11 GPa at  $T = 77$  K to 1 GPa at  $T = 1800$  K. On the other hand, we find an increase in  $\partial z / \partial p$  with increasing temperature at constant load. We conclude that Young's modulus  $Y$ , defined by  $Y = \partial p / \partial z$ , decreases as the temperature rises. Both effects indicate that the material becomes softer and easily deformable with increasing temperature, which agrees with our everyday experience. Microscopically, this softening corresponds to the increased probability of activated atomic diffusion leading to a new equilibrium geometry (plastic deformations to a "thin wire" and fracture under excessive uniaxial load). In the elastic region  $p \ll p_c$ , the  $\Delta z$ - $p$  relationship is nearly lin-

ear for all temperatures. This Hooke's-law-type behavior is expected based on our interaction potential which is dominated by harmonic terms close to the equilibrium.

It is interesting to note that our above MD simulations, performed under *uniaxial* stress, contain the information about the bulk modulus  $B$  which describes the elastic response to *isotropic pressure*. For a cubic crystal, the elastic response to a very small applied uniaxial stress  $p$  is

$$p = C_{11}\epsilon_1 + 2C_{12}\epsilon_2 \quad (10)$$

along the direction of the load. Here,  $\epsilon_1$  and  $\epsilon_2$  are the strain components along the load direction and perpendicular to the load direction, respectively, and  $C_{11}$  and  $C_{12}$  are elastic stiffness constants. No stress occurs perpendicular to the load direction [see Fig. 4(a)], so

$$0 = C_{12}\epsilon_1 + C_{11}\epsilon_2 + C_{12}\epsilon_2. \quad (11)$$

From Eqs. (10) and (11) we get

$$p = (C_{11} + 2C_{12}) \frac{V(p) - V(p=0)}{V(p=0)}. \quad (12)$$

Using  $B = (1/3)(C_{11} + 2C_{12})$  for a cubic crystal, we finally get

$$B = \frac{1}{3} V \left( \frac{\partial V}{\partial p} \right)_{p=0}^{-1}. \quad (13)$$

As shown in Fig. 5(a), our results for the absolute value of  $B$  and the temperature dependence of  $B$  are in good

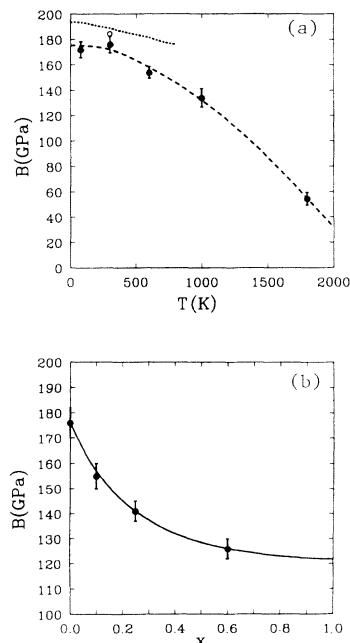


FIG. 5. (a) Temperature dependence of the bulk modulus  $B$  of Pd. The dashed line is a guide to the eye connecting the calculated points, given by solid circles. The dotted line shows the experimental data of Ref. 25. (b) Dependence of the bulk modulus of  $\text{PdH}_x$  on the hydrogen concentration  $x$ .

agreement with the experimental data of Ref. 25. At low temperatures, we find the bulk modulus to be essentially independent of temperature. With rising temperature, however, our results indicate a strong decrease of  $B$ .

We found it instructive to inspect the distribution of binding energies for a signature of atomic fracture at very large tensile loads. In Fig. 3(c), we show the distribution at the point of critical tensile stress  $p_c$ , for a developed fracture. As compared to the stress-free situation shown in Figs. 3(a) and 3(b), the distribution of binding energies shows several distinctive peaks. The lowest binding energies correspond to sites at the surface of the crack and the highest binding energies, the same as in the stress-free sample shown in Fig. 3(a), correspond to bulk sites in the intact fragments.

### C. Mechanical stability of H-loaded Pd under tensile stress

Hydrogen is well known to dissociate at transition metal surfaces and to penetrate easily into the bulk metal, releasing the heat of hydride formation in many systems such as Pd.<sup>1</sup> This process makes such metals an ideal medium for hydrogen storage. On the other hand, the presence of hydrogen is known to have an adverse effect on mechanical properties of metals, specifically facilitating the formation of cracks under tensile stress.<sup>2</sup> In order to obtain a microscopic understanding of the processes associated with hydrogen-assisted crack formation, we simulated the response of hydrogen-loaded Pd to uniaxial tensile stress in a molecular-dynamics calculation.

We have chosen a cubic simulation box containing 500 Pd atoms as the initial MD unit cell, and occupied the 500 octahedral interstitial sites in the lattice at random with hydrogen atoms. We have considered three different H concentrations in PdH $_x$ , namely,  $x = 0.1, 0.25$ , and  $0.6$ , and performed all simulations at room temperature,  $T = 300$  K. At each H concentration, we first let the system equilibrate over a period of more than 30 000 time steps (corresponding to  $1.5 \times 10^{-11}$  s).

First, we study the volume changes due to hydrogen at zero pressure. The free volume  $V(x)$  of Pd atoms in PdH $_x$ , shown in Fig. 1(b), has been determined for each H concentration  $x$  by averaging over 10 000 time steps after reaching the equilibrium. We found the free volume to increase almost linearly with increasing hydrogen concentration  $x$ , which agrees with the observed relation<sup>23</sup>  $V(x) = V(0)(1 + 0.19x)$ .

In order to understand the effect of dissolved hydrogen on the mechanical stability of Pd, we studied the response of the system to uniaxial tensile stress using molecular dynamics. As in the hydrogen-free samples, we first allowed the system to equilibrate under fixed external tensile stress  $p$  and kept the temperature of the heat bath constant at  $T = 300$  K. Then, we determined the stress-induced elongation  $\Delta z$  of the simulation box by averaging over 10 000 time steps (corresponding to  $5 \times 10^{-12}$  s). Our results, presented in Fig. 4(c), show an almost linear relationship between  $p$  and  $\Delta z$ . We found the slope of the  $\Delta z(p)$  curves to be almost independent of  $x$  at low values of  $p$ , indicating that changes of the hy-

drogen concentration have little effect on Young's modulus  $Y$ . Our results also indicate that the critical tensile stress  $p_c$  for the onset of fracture, corresponding to the "end points" of the  $\Delta z(p)$  curves, decreases with increasing hydrogen concentration. We find that hydrogen can reduce the critical tensile stress for fracture  $p_c$  substantially when compared to the hydrogen-free system, but that the order of magnitude of  $p_c$  in the different systems is the same. This hydrogen-induced reduction of the mechanical strength is sometimes called "hydrogen embrittlement."<sup>2</sup> As we discuss later on, our microscopic results indicate that this is a misnomer; we find hydrogen to enhance the *ductility* and *plasticity* of the metal matrix locally, thereby weakening the structure as a whole.

We can also use our MD calculations for *uniaxial* tensile stress to estimate the bulk modulus of the system, following the procedure outlined in the preceding subsection. Our results, presented in Fig. 5(b), indicate that the bulk modulus  $B$  decreases strongly in the presence of hydrogen. Another quantity of interest is the Poisson's ratio  $\mu$  which is the ratio of the unit cell deformations along the direction of the applied load  $\Delta z$  and perpendicular to it  $\Delta x$ . In a cubic system,  $\mu$  relates Young's modulus and the bulk modulus as  $B = Y/(3 - 6\mu)$ , which defines  $\mu$  as

$$\mu = \frac{1}{2} - \frac{Y}{6B}. \quad (14)$$

Our above results for  $Y(x)$  and  $B(x)$  indicate that Poisson's ratio decreases strongly with increasing hydrogen concentration in the metal.

As in the hydrogen-free system, we investigated the distribution of binding energies for a signature of atomic fracture at different tensile loads. Our results for the PdH $_{0.25}$  system are summarized in Fig. 6(a) for zero

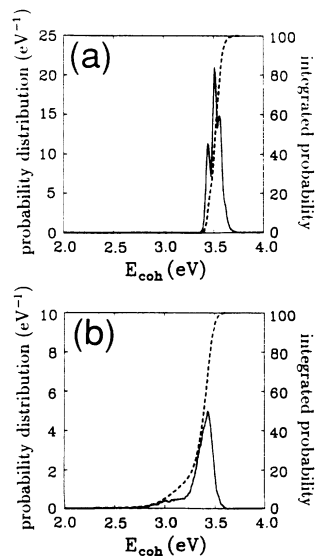


FIG. 6. Distribution of binding energies of Pd atoms  $E_{\text{coh}}(\text{Pd})$  in bulk PdH $_{0.25}$  at  $T = 300$  K (a) at zero pressure and (b) at the point of critical uniaxial tensile stress  $p_c$  [compare with Fig. 4(c)]. The solid lines give the probability distribution; the dashed lines show the integrated probability.

tensile stress and in Fig. 6(b) for critical tensile stress. The structure of the binding energy distribution in the stress-free case reflects the distribution of inequivalent Pd atoms with 0–6 H nearest neighbors. The relatively featureless distribution of binding energies at the point of critical tensile stress  $p = p_c$ , displayed in Fig. 6(b), is in sharp contrast to the hydrogen-free case shown in Fig. 3(c), and is more reminiscent of the results for molten Pd, shown in Fig. 3(b). The absence of distinct fracture-related features in the binding energy distribution in Fig. 6(b) indicates that all Pd atoms reside in a relatively homogeneous atomic environment. This environment is close to the molten system; it has an amorphous structure and can easily be plastically deformed. We conclude that increased hydrogen concentration has a similar effect on the mechanical properties of Pd as a temperature increase, namely, an increased ductility and plasticity.

An independent microscopic signature of fracture on the atomic scale can be often found in the distribution of Wigner-Seitz volumes associated with the individual atoms in the crystal. The statistical presence of large atomic volumes indicates the occurrence of fracture with no additional assumptions about the number, position, or morphology of one or more simultaneous cracks. This information is displayed in Fig. 7 for Pd and H atoms in PdH<sub>0.25</sub> at  $p = p_c$ . The volumes of Pd atoms, given by the solid line, show a distribution which is characterized by a sharp peak near 15 Å<sup>3</sup>, corresponding to atoms in bulklike environment, and a wide structureless tail towards larger volumes, associated with atoms near the crack surface. This finding again confirms our previous conclusion that Pd atoms have no preferential binding arrangement in the hydrogen-loaded sample, which shows a plastic behavior under critical tensile stress.

The preferential *hydrogen* sites in this structure are determined in the following way. We enlarged the original Wigner-Seitz volumes of Pd atoms by a factor of 1.5 in

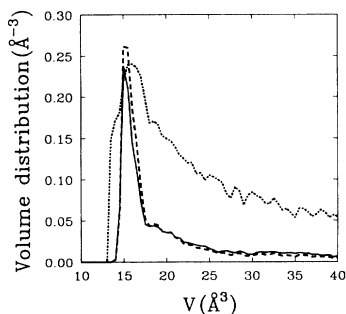


FIG. 7. Distribution of atomic volumes in bulk PdH<sub>0.25</sub> at  $T = 300$  K. The solid line shows the distribution of atomic volumes associated with Pd atoms, obtained using the Wigner-Seitz cell construction. The dashed line is obtained by first determining which Pd sites are associated with each of the H atoms in the lattice, and displaying the distribution of these Pd volumes. The dotted line gives the ratio of the values given by the dashed and the solid lines, divided by the volume and multiplied by 3.

each direction and for each hydrogen atom in the crystal; we generated a list of Pd sites which contain this atom in their enlarged unit cell. This definition allows for more than one Pd site to be associated with a given hydrogen atom. Next, we combined the lists of Pd sites associated with each H atom and plotted the distribution of the corresponding Pd Wigner-Seitz volumes. The results are given by the dashed line in Fig. 7. A comparison with the solid line for the Pd atoms shows no strong preference of hydrogen atoms for specific sites in the metal structure. The dotted line in Fig. 7 represents the probability that a Pd atom, characterized by its atomic volume, is likely to have one or more hydrogen atoms as its closest neighbors. In case that there would be no preferential sites for hydrogen atoms, this curve should be flat. Our results indicate a strong preference of hydrogen atoms for sites near highly coordinated Pd atoms in the bulk. From the position of the peak in the dotted curve, which lies at a slightly larger volume than that of bulk Pd atoms, we infer that hydrogen atoms are more likely to occupy subsurface sites or sites close to the crack tip than sites in the bulk of Pd.

#### IV. DISCUSSION

Our molecular-dynamics calculations, based on the Nosé and Rahman-Parrinello formalism, provide us with a useful and consistent picture of the atomic-scale processes which occur in PdH<sub>x</sub> at different temperatures and hydrogen concentrations  $x$ , specifically in response to large uniaxial tensile stress. Even though our interaction potentials are obtained from static  $T = 0$  *ab initio* calculations, the finite temperature results of our simulations are in good agreement with experimental data. This increases our confidence that the MBA Hamiltonian describes the interactions in the Pd-H system correctly to a large degree. Since this Hamiltonian has a solid theoretical background, it can provide microscopic insight into the nature of interatomic interaction under different conditions.

Our simulations show that the introduction of hydrogen into bulk Pd at room temperature has a similar effect on the structural properties and elastic behavior as a temperature increase in the hydrogen-free metal. Increased hydrogen loading and increased temperature both increase the free volume linearly, decrease the bulk modulus, and reduce the critical tensile stress for fracture. It is plausible to some degree that the presence of hydrogen simulates a temperature increase, since the light H atoms have a much faster dynamics than Pd atoms and can easily excite Pd vibrations in elastic collisions. This effect is enhanced by the fact that hydrogen atoms reduce the bonding strength between Pd atoms and soften the vibrational modes of the Pd lattice.<sup>8</sup> We find that hydrogen-induced changes of structural properties and elastic response increase with increasing  $x$ , as shown in Figs. 1(b), 5(b), and 4(c). At the point of fracture, we find that the presence of hydrogen enhances the plasticity of the system significantly, causing hydrogen-assisted “melting” even at  $T = 300$  K, which is associated with

a substantial diffusion of Pd atoms. We found it useful to compare our results for hydrogen-loaded Pd under critical tensile stress to hydrogen-free Pd at the melting point in an animated video movie, and found Pd diffusion at the crack surface of the hydrogen-loaded system to be comparable with the atomic diffusion in melting Pd metal.

As mentioned above, a fundamental difference between the effect of hydrogen loading and temperature increase lies in the fact that hydrogen modifies the interaction between Pd atoms. This difference is most obvious in the response to uniaxial tensile stress, shown in Figs. 4(b) and 4(c). In the hydrogen-free system, we observe both the bulk and Young's moduli to decrease with increasing temperature, while Poisson's ratio  $\mu$  is nearly constant, consistent with Eq. (14). On the other hand, increasing the hydrogen concentration in Pd at a constant temperature  $T = 300$  K still causes the bulk modulus to decrease, but has little effect on Young's modulus. In this case, Poisson's ratio decreases with increasing hydrogen loading, indicating an increasing resistance against shape deformations. This effect could also assist in the initial formation of cracks. Based on our results shown in Fig. 4(c), we find that the critical values of tensile stress  $p_c$  drop at an increasing rate with increasing hydrogen concentration, indicating a continuous reduction of the Pd-Pd bond strength with increasing number of H atoms in the vicinity of the metal bonds.

The microscopic origin of the reduced Pd-Pd bond strength in the presence of hydrogen is the rehybridization of Pd orbitals in the hydrogen-loaded metal. As we found in our previous *ab initio* calculation of atomic binding in bulk Pd and PdH,<sup>10</sup> the hydrogen-induced decohesion of Pd stems mainly from a filling of antibonding states in the Pd4d band, accompanied by a depletion of the partly filled Pd5s band and a small charge transfer towards hydrogen. These effects are considered, albeit in a very approximate way, in our many-body alloy Hamiltonian. Unlike in models based on pairwise interactions, we do consider the different electronic hopping processes to neighboring atoms from the point of view of electronic band formation when calculating the attractive part of our total energy. Hence the binding energy of a Pd atom is not simply proportional to the number of nearest neighbors, but depends in a more complex way on the hybridization with the neighboring atoms and the band filling, which appears to be essential for the understanding of bonding changes in this system.

Our calculated values for the critical tensile stress are about one order of magnitude too high when compared to experimental data for single and polycrystalline samples. There are two reasons which cause this overestimate of  $p_c$ . First, it is impossible to study the dynamics of the fracture process in a molecular-dynamics calculation for realistic time scales and large systems. The time spans presently accessible by such simulations fall at least ten orders of magnitude short of a realistic time for the formation of a crack, which is typically seconds. Second, in a realistic system, the fracture process is assisted and proceeds by dislocation motion in the crystal. Our unit cell containing 500 Pd atoms, which is large for MD stan-

dards, is clearly too small to show the spontaneous formation and motion of dislocations.

We addressed the effect of dislocations in a somewhat artificial way, namely, removing a single atom from the unit cell, thus creating a defect site and a possible seed for a dislocation or a crack. The corresponding MD simulation did not show a reduction of  $p_c$  as compared to the initially "perfect" systems. Obviously, the typical atomic fluctuations near the point of fracture are large and comparable to the size of a single atomic vacancy.

In hydrogen-loaded Pd, the local decohesion and structural relaxations are mediated by hydrogen which has a very large diffusion constant. We studied the interplay between the time scales for structural changes and the diffusion of hydrogen by considering isotope substitution. We found that replacing H by D atoms in PdH<sub>x</sub> has no effect on  $p_c$ , probably due to the large difference between the time scales for hydrogen motion and structural relaxation, and possibly also the incoherent motion of hydrogen atoms in the metal which averages out local changes of elastic properties.

Our microscopic results for the elastic response of hydrogen-loaded Pd under uniaxial tensile stress strongly support one of the previously postulated mechanisms for "hydrogen embrittlement," namely, the hydrogen-enhanced local-plasticity (HELP) mechanism.<sup>26</sup> This mechanism, which has been used to interpret experimental data, postulates that hydrogen concentrates preferentially near the tip of a starting crack. Hydrogen subsequently locally softens the metal matrix in the vicinity of the crack tip, which leads to an increase in the velocity of dislocation motion. This process can lead to a softening over microns over very short time scales. The system will become microscopically ductile, but will appear as brittle on macroscopic length scales.

While our calculations have been performed for a specific system, namely hydrogen loaded Pd, we expect that the effect of hydrogen on the stability of other fcc metals will be qualitatively the same. The situation in bcc metals (such as Fe) may be somewhat different, since hydrogen is observed to stiffen rather than soften these structures.<sup>26</sup> These questions are presently being addressed in corresponding MD simulations.<sup>27</sup>

## V. SUMMARY AND CONCLUSIONS

We have used the Nosé and Rahman-Parrinello molecular dynamics formalism to study the equilibrium structure and elastic properties of bulk Pd as a function of temperature and hydrogen concentration. The interatomic interaction in the Pd-H system has been described by a many-body alloy Hamiltonian based on *ab initio* density-functional calculations. We have used this formalism first to predict the elastic constants, thermal expansion, and melting temperature of hydrogen-free bulk Pd. We found our results to be in good agreement with available experimental data.

Introducing uniaxial tensile stress as an independent variable into this formalism has enabled us also to study the elastic deformations as a function of the applied load at different temperatures and hydrogen concentrations.

At small applied loads, we found that the bulk and Young's moduli decrease with increasing temperature in hydrogen-free bulk Pd. Increased hydrogen concentration at constant temperature has a very similar effect as the temperature increase in the hydrogen-free metal: The system gets softer, which is reflected in a decreased bulk modulus. While hydrogen softens the Pd-Pd bonds, its presence does not affect Young's modulus. Consequently, Poisson's ratio decreases with increasing hydrogen loading, indicating an increasing resistance against shape deformations. This behavior might assist in the formation of cracks.

At large values of the uniaxial tensile stress, we observe the onset of crack formation. We find that the critical tensile stress for fracture decreases both with increasing temperature and increasing hydrogen concentration. Near the point of fracture, however, the elastic response of hydrogen-free and hydrogen-loaded Pd are vastly different. Following the fracture, Pd atoms can be found in well-defined sites in the ordered bulk of the fragments or at the crack surface in Pd which is free of hydrogen. In hydrogen-loaded Pd, no such well-defined sites exist any more at the point of frac-

ture. We rather find a broad distribution of Pd sites in an amorphous system which can easily be deformed plastically. We conclude that the hydrogen-induced reduction of the mechanical stability of Pd (and likely also other metals) originates from an increased *ductility* and *plasticity* in parts of the sample with a large hydrogen concentration, such as regions near grain boundaries and dislocations. These conclusions agree with one of the previously postulated mechanisms for "hydrogen embrittlement," namely, the hydrogen-enhanced local-plasticity mechanism.<sup>26</sup> More detailed studies will be necessary to confirm this behavior also in bcc metals (such as iron). A comparison with corresponding experimental studies, preferentially on single crystals and showing atomic resolution, would be highly desirable.

#### ACKNOWLEDGMENTS

We thank Dr. Sean Y. Li, Dr. Gregor Overney, and Professor Howard Birnbaum for useful discussions and helpful comments. This work has been supported by the Office of Naval Research under Contract No. N00014-90-J-1396. CONVEX computer time has been provided by a grant from Michigan State University.

\*Present address: Department of Physics and Astronomy, Rutgers University, P.O. Box 849, Piscataway, NJ 08855-0849.

<sup>†</sup>Electronic address: TOMANEK@MSUPA.bitnet, tomanek@msupa.pa.msu.edu

<sup>1</sup>*Hydrogen in Metals I and II*, Topics in Applied Physics, Vols. 28 and 29, edited by G. Alefeld and J. Völkl (Springer-Verlag, Berlin, 1978).

<sup>2</sup>H.K. Birnbaum, M. Grossbeck, and S. Gahr, in *Hydrogen in Metals*, edited by M. Bernstein and A. Thompson (American Society for Metals, Metals Park, OH, 1973), p. 303; H.K. Birnbaum, in *Environmentally Sensitive Fracture of Engineering Materials*, edited by Z. A. Foroulis (T.M.S., New York, 1979), p. 326.

<sup>3</sup>A.A. Maradudin, E.W. Montroll, and G.H. Weiss, *Theory of Lattice Dynamics in the Harmonic Approximation* (Academic, New York, 1963).

<sup>4</sup>M.P. Allen and D.J. Tildesley, *Computer Simulation of Liquids* (Oxford, New York, 1990); A.E. Carlsson, in *Solid State Physics* (Academic, New York, 1990), Vol. 43, p. 1.

<sup>5</sup>K.-M. Ho and K.P. Bohnen, Phys. Rev. Lett. **56**, 934 (1986).

<sup>6</sup>M.S. Daw and M.I. Baskes, Phys. Rev. B **29**, 6443 (1984); S.M. Foiles, *ibid.* **32**, 3409 (1985); Surf. Sci. **191**, L779 (1987); M.S. Daw, Phys. Rev. B **39**, 7441 (1989); S.M. Foiles and J.B. Adams, *ibid.* **40**, 5909 (1989).

<sup>7</sup>L.R. Pratt and J. Eckert, Phys. Rev. B **39**, 13 170 (1989); P. Stoltze, J.K. Nørskov, and Uzi Landman, Surf. Sci. Lett. **220**, L693 (1989); Liqiu Yang, Talat S. Rahman, and Murray S. Daw, Phys. Rev. B **44**, 13 725 (1991).

<sup>8</sup>W. Zhong, Y.S. Li, and D. Tománek, Phys. Rev. B **44**, 13 053 (1991).

<sup>9</sup>D. Tománek, S.G. Louie, and C.T. Chan, Phys. Rev. Lett. **57**, 2594 (1986).

<sup>10</sup>Z. Sun and D. Tománek, Phys. Rev. Lett. **63**, 59 (1989).

<sup>11</sup>D. Tománek, Z. Sun, and S.G. Louie, Phys. Rev. B **43**, 4699 (1991).

<sup>12</sup>D. Tománek, S. Mukherjee, and K.H. Bennemann, Phys. Rev. B **28**, 665 (1983); **29**, 1076 (1984) (E).

<sup>13</sup>D. Tománek, Phys. Lett. **113A**, 445 (1986); D. Tománek and K.H. Bennemann, Surf. Sci. **163**, 503 (1985).

<sup>14</sup>D. Tománek, A.A. Aligia, and C.A. Balseiro, Phys. Rev. B **32**, 5051 (1985).

<sup>15</sup>D. Spanjaard and M.C. Desjonquères, Phys. Rev. B **30**, 4822 (1984).

<sup>16</sup>W. Zhong, G. Overney, and D. Tománek (unpublished).

<sup>17</sup>S. Nosé, J. Chem. Phys. **81**, 511 (1984); Mod. Phys. **52**, 255 (1984).

<sup>18</sup>H.C. Andersen, J. Chem. Phys. **72**, 2384 (1980).

<sup>19</sup>M. Parrinello and A. Rahman, Phys. Rev. Lett. **45**, 1196 (1980); J. Appl. Phys. **52**, 7182 (1981); J. Chem. Phys. **76**, 2662 (1982); J.R. Ray and A. Rahman, *ibid.* **80**, 4423 (1984); J.R. Ray, Comp. Phys. Rep. **8**, 109 (1988).

<sup>20</sup>C.W. Gear (private communication).

<sup>21</sup>D. Kusnezov, A. Bulgac, and W. Bauer, Ann. Phys. **204**, 155 (1990).

<sup>22</sup>W.B. Pearson, *A Handbook of Lattice Spacings and Structures of Metals and Alloys* (Pergamon, New York, 1958).

<sup>23</sup>H. Peisl, in *Hydrogen in Metals I*, Topics in Applied Physics, Vol. 28, edited by G. Alefeld and J. Völkl (Springer-Verlag, Berlin, 1978), p. 69.

<sup>24</sup>Ch. Kittel, *Introduction to Solid State Physics*, 6th ed. (Wiley, New York, 1986).

<sup>25</sup>*Landolt-Börnstein (New Series) Handbook of Numerical Data and Functional Relationships in Science and Technology*, edited by K.-H. Hellwege, Group III, Vol. 11 (Springer-Verlag, New York, 1979), pp. 10 and 114.

<sup>26</sup>Howard K. Birnbaum (private communication).

<sup>27</sup>W. Zhong and D. Tománek (unpublished).

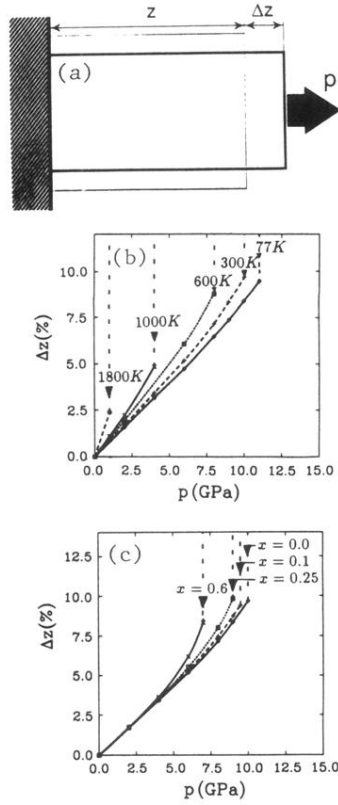


FIG. 4. (a) Schematic picture of Pd deformations under tensile stress, showing the length  $z$  and deformation  $\Delta z$  of the unit cell. (b) Deformation  $\Delta z$  of bulk Pd as a function of the external tensile stress  $p$ , for different temperatures. (c) Deformation  $\Delta z$  of hydrogen-loaded bulk Pd at  $T = 300$  K, as a function of the external tensile stress  $p$ , for different hydrogen concentrations. Our molecular dynamics results are given by the data points. The lines are guides to the eye.